Depumping a Sr magneto-optical trap via 5s5d $^1D_2$

Scott Wolzak

Bachelor Thesis Physics & Astronomy
Date of submission: July 19, 2021

Student ID	11906944
Supervisor	Prof. Dr. Florian Schreck
Daily Supervisors	Ivo Knottnerus MSc & Dr. Benjamin Pasquiou
Second Examiner	Dr. Klaasjan van Druten
Bachelor	Physics & Astronomy (Joint Degree UvA/VU)
University	University of Amsterdam & VU University Amsterdam
Institute	Van der Waals-Zeeman Institute (WZI)
Faculty	Faculteit der Natuurwetenschappen, Wiskunde en Informatica (FNWI)
Project Duration	09-04-2021 to 25-06-2021





Abstract

During this bachelor project a magneto-optical trap (MOT) of ^{88}Sr was depumped on the 5s5p $^1P_1$ - 5s5d $^1D_2$ transition. To make this possible, an optical setup was created that provided light with the transition frequency to the atoms inside the MOT. The transition frequency was determined to be 390.59962(2) THz, by measuring the blue MOT fluorescence during a depump laser frequency sweep. Absorption imaging was used to determine the number of atoms inside the MOT. The observed atom number increase was by a factor of 4.0(3) for blue detuned light at 390.59964(1) THz. The depumping intensity that produced maximal atom number enhancement, with a factor of 4.6(2), was measured at 0.9(3) mW / cm^2 $\approx 3\ I_{sat}$. The loading rate of atoms into the $^3P_2$ state was observed to increase by a factor of 3.6. This thesis provides a possible explanation for this observed increase in atom number.

Populair Wetenschappelijke Samenvatting

Alles in de wereld om ons heen is opgebouwd uit kleine deeltjes, namelijk atomen. Deze atomen vormen de bouwstenen van zowel vloeistoffen als vaste stoffen, ook de mens bestaat uit een hele hoop atomen. Er zijn verschillende soorten atomen, dit zijn de elementen uit het periodiek systeem. Het atoom bestaat zelf ook weer uit nog kleinere deeltjes: protonen en neutronen in de atoomkern met daar omheen bewegende elektronen.

De elektronen zijn om de atoomkern verdeeld in specifieke banen, dit noemt met de elektronenconfiguratie. Deze configuratie van de elektronen bepaalt het energieniveau van het atoom. Om een elektron in een baan verder van de atoomkern te krijgen moet er energie aan het atoom worden toegevoegd. Een elektron dat zich al in een baan ver van de kern bevindt kan terug vallen naar een baan dichter bij de kern door energie te verliezen, in de vorm van licht. De energieniveaus van verschillende elektronenconfiguraties zijn discreet, dat wil zeggen dat het energie verschil tussen energieniveaus niet alle waarden kan aannemen. Alleen als er precies de juiste hoeveelheid energie wordt toegevoegd is er een overgang mogelijk naar de nieuwe elektronenconfiguratie. Door licht met exact deze energie op het atoom te schijnen, kan de overgang plaatsvinden.

De temperatuur van atomen wordt bepaald door hoe snel ze heen en weer bewegen. Een atoom dat helemaal stil staat heeft dan een temperatuur van nul, aangezien het niet langzamer kan dan stil staan. Deze laagst mogelijke temperatuur noemt men het absolute nulpunt en bedraagt 0 Kelvin, dat is -273.15° Celcius. Bij kamertemperatuur kunnen atomen sneller gaan dan 400 meter per seconde, sneller dan de geluidssnelheid. Door atomen enorm af te koelen tot dat ze bijna stil staan, kan beter worden bestudeerd hoe de natuur werkt op de kleinste schaal. Het afkoelen van atomen wordt gedaan met licht.

Wanneer licht met de juiste energie schijnt op een atoom dat richting de lichtbron beweegt, kan het atoom het licht absorberen. Hierdoor krijgt het atoom een hoger energieniveau en zal de impuls van het licht worden overgedragen aan die van het atoom. Zo wordt het atoom afgeremd en dus gekoeld. Dit kun je vergelijken met een biljartbal die op een andere bal botst, waarbij de impuls van de ene bal wordt overgedragen aan de ander. Door licht te combineren met een magneetveld, kunnen atomen zelfs worden ‘gevangen’ op één positie, in wat een magnetisch-optische val wordt genoemd.

Dit onderzoek richt zich op atomen van het element strontium die worden gevangen en gekoeld in een magnetisch-optische val. Na het koelen in de magnetisch-optische val, vallen de atomen terug naar een lager energieniveau dat bijna stabiel is. De atomen blijven wel honderden seconden in deze toestand, terwijl de meeste toestanden in een paar miljardsten van een seconde vervallen naar een lager energieniveau. Doordat deze toestand bijna stabiel is, kunnen er goed experimenten mee worden gedaan. Een nadeel is alleen dat het lang duurt voordat de atomen in de bijna stabiele toestand komen, wat er voor zorgt dat één experimentele cyclus enkele seconden duurt. Als het experiment vaak moet worden herhaald kost dit veel tijd. Het doel van dit project is om te kijken of de experimentele cyclus, waarbij strontium atomen in de bijna stabiele toestand komen, kan worden versneld.

Door laserlicht met een golflengte van 767.5 nm te schijnen op de strontium atomen in de magnetisch-optische val, is het gelukt om atomen sneller in de bijna stabiele toestand te krijgen en dus de experimentele cyclus efficiënter te maken.

Contents

1 Introduction **7**

1.1 The History of Ultracold Atoms . . . 7
1.2 Modern Research . . . 7
1.3 Project Objective . . . 7
1.4 Thesis Overview . . . 8

2 Theoretical Background **8**

2.1 Atomic Properties of Strontium . . . 8
2.2 Laser Cooling . . . 9
2.2.1 Cooling Limits . . . 9
2.2.2 Scattering Rate & Power Broadening . . . 10
2.3 Magneto-Optical Trap . . . 11
2.3.1 Magnetic Quadrupole Field . . . 11
2.3.2 Optical Molasses . . . 12
2.3.3 Zeeman Effect . . . 12
2.4 Energy Levels and Transitions . . . 13
2.4.1 Cooling Transitions . . . 13
2.4.2 Leaking into the $^3P_2$ reservoir . . . 13
2.4.3 Repumping the $^3P_2$ reservoir . . . 14
2.5 Depumping towards 5s5d $^1D_2$ . . . 14

3 Methodology & Setup **16**

3.1 Laser System . . . 16
3.1.1 External-Cavity Diode Laser . . . 16
3.1.2 Wavelength Tuning . . . 17
3.1.3 Laser Characteristics . . . 17
3.2 Optical Isolator . . . 20
3.3 Optical Fibers & Collimators . . . 21
3.4 Optimising Beam Shape . . . 22
3.4.1 Beam Waist & Intensity Distribution . . . 23
3.4.2 Cylindrical Optics . . . 23

4 Results **25**

4.1 Blue MOT Fluorescence . . . 25
4.2 Atom Number Enhancement . . . 27
4.3 Optimal Depumping Intensity . . . 28

4.4 Loading Time Enhancement 29

5 Discussion **31**

5.1 Transition Frequency 31

5.2 Atom Number Enhancement 31

5.3 Loading Time Enhancement 33

6 Conclusion & Outlook **33**

Acknowledgements **35**

References **36**

1 Introduction

1.1 The History of Ultracold Atoms

At the start of the 20th century, it was already known that light could exert a force in the form of radiation pressure. In 1933 Otto Frisch observed that individual sodium atoms were deflected by resonant light from a sodium-vapor lamp [1]. In the 1970s, physicists explored new ways of atom manipulation using the recent invention of the laser. This led to the first proposals for *laser cooling* in 1975, by two research groups at the same time: the group of Wineland & Dehmelt [2] and second the group of Hänsch & Schawlow [3]. Soon after laser cooling was proposed, laser light was used to optically trap and cool atoms simultaneously. This gave rise to a new field in physics, that of ultracold atoms.

A major advancement in the field of ultracold atoms was made by Raab *et al.* with the development of the magneto-optical trap in 1987 [4]. This trap would allow for relatively long spectroscopic measurements of samples of ultracold atoms and provide a platform to study the interaction between atoms. The cooling techniques developed in the field of ultracold atoms led to the realisation of a *new state of matter*, known as a Bose-Einstein condensate, for which Cornell, Wieman, and Ketterle received the Nobel prize in 2001 [5]. The following section will highlight some of the modern ultracold atom experiments that take place in the strontium quantum gas group.

1.2 Modern Research

The strontium quantum gas group, led by Prof. Dr. Florian Schreck, is part of the Van der Waals-Zeeman institute (WZI) and is hosted at the University of Amsterdam (UvA). In the laboratories of the research group, various projects with ultracold strontium atoms are conducted. These projects include: quantum computing and simulation using Rydberg coupled strontium atoms in optical tweezer arrays (SrMIC), creating a quantum gas of RbSr-molecules, building a continuous atom laser (SrPAL), and making a superradiant atomic clock (iqClock) [6]. The research conducted in this bachelor project took place at the SrMIC laboratory of the strontium quantum gas group.

1.3 Project Objective

The experimental cycle to cool strontium atoms uses a magneto-optical trap (MOT), from which atoms slowly decay into a magnetically trappable $^3P_2$ state. This state has several properties that make it ideal for experiments exploring quantum physics. However, since the decay into

this state is slow, the experimental cycle requires a long loading time.

The aim of this bachelor project is to accelerate the loading of strontium atoms into the magnetically trappable $^3P_2$ state by depumping the strontium MOT on the 5s5p $^1P_1$ - 5s5d $^1D_2$ transition. In addition, the effect of depumping on the number of atoms in the MOT will be measured.

1.4 Thesis Overview

This thesis will start off by providing theoretical background information about the project in section 2. Subsequently, the optical setup that was used in the experiment will be introduced in section 3 and highlights of the individual components that make up the optical setup is given in the following subsections. The results of the project are shown in section 4 and are discussed in section 5, in which a possible explanation is given for the observed results. The thesis concludes with a summary of the project results in section 6 and provides an outlook for future research that involves depumping strontium on the 5s5p $^1P_1$ - 5s5d $^1D_2$ transition.

2 Theoretical Background

2.1 Atomic Properties of Strontium

Strontium is an alkaline-earth metal with atomic number $Z = 38$. Alkaline-earth metals share the property of having a full outer s-orbital with two valence electrons. There exist both singlet and triplet electronic states for strontium, due to the spin orientation of the valence electrons. The electronic ground state configuration of strontium is given by: [Kr]$5s^2$ with term symbol $^1S_0$.

Strontium has four stable isotopes, three of which are bosonic (^{84,86,88}Sr) and one is fermionic (^{87}Sr). The bosonic ^{88}Sr isotope is the most abundant in nature and was used in this experiment. An overview of the natural abundance of each isotope given in table (1). This experiment is conducted using bosonic ^{88}Sr.

An important property of strontium is the existence of metastable states. Metastable states have a relatively long lifetime in the realm of atomic transitions. For strontium the $^3P_0$ and $^3P_2$ states are metastable *triplet* states and thus require a spin-flip to decay towards the $^1S_0$ *singlet* ground state. A spin-flip cannot be performed by the emission of a single photon, which makes

Isotope	Mass	Abundance (%)	Statistics	Nuclear spin
^{84}Sr	83.913430	0.56	Bosonic	0
^{86}Sr	85.909267	9.86	Bosonic	0
^{87}Sr	86.908884	7.00	Fermionic	9/2
^{88}Sr	87.905619	82.58	Bosonic	0

Table 1: Properties of naturally occurring isotopes of strontium [7].

these states stable in theory [8]. In practise however, due to higher order decay mechanisms, the lifetime of the $^3P_0$ and $^3P_2$ metastable states is on the order of hundreds of seconds [9]. The $^3P_2$ state has besides a long lifetime, also a magnetic moment and as a result the low-field seeking $m_j = 2, 1$ states are magnetically trappable. This makes the $^3P_2$ state ideal for ultracold atom experiments.

2.2 Laser Cooling

Laser cooling is used to cool atoms or molecules down to temperatures near quantum degeneracy. Several different laser cooling techniques exist, but they mostly rely on the same principle, *Doppler cooling*: When atoms move towards a light source that is *red detuned*, with a frequency slightly below an electronic transition, the atoms will absorb more photons since the Doppler effect shifts the frequency towards resonance. Now, when an atom absorbs a photon that carries momentum from the counterpropagating beam, it will re-emit a photon in a random direction, which changes the momentum of the atom by conservation of momentum. Since the re-emission of a photon is isotropically distributed, on average the momentum change will equal the momentum of the initial photon, effectively slowing the atom down. Since the kinetic energy of the atom is reduced, this is equivalent to cooling the atom.

2.2.1 Cooling Limits

Unfortunately, there are limits that prevent arbitrarily low temperatures to be reached using laser cooling. An atom that emits a photon with momentum $p = \hbar k$ will recoil after the emission, the recoil velocity of the atom is given by

$$v_r = \frac{\hbar k}{M}, \tag{1}$$

where $\hbar$ is the reduced Planck constant and M denotes the mass of the atom [10]. The change in velocity by recoil from a single photon emission is only a few cm/s, so many absorption-emission cycles are necessary to produce a large velocity change. The recoil velocity defines the lowest

temperature that can be achieved with laser cooling methods for which the interaction between the cooled atoms and light is permanent. This lower limit on temperature due to atomic recoil is defined as the recoil limit and is defined as

$$T_r = \frac{\hbar^2 k^2}{M k_B}, \tag{2}$$

where k_B is the Boltzmann constant [10]. Beside the recoil limit, another limit arises from fluctuations in atom velocity, namely, the Doppler limit T_D. As mentioned previously, the spontaneous emission of photons is isotropic and thus provides on average a zero velocity change to the atom $\langle v \rangle = 0$. But the mean velocity squared $\langle v^2 \rangle$ is non zero, such that energy or heat is provided to the atom with velocity fluctuations. The equilibrium between heating and cooling rate defines the Doppler limit, the amount an atom can be cooled using an atomic transition, given by

$$T_D = \frac{\hbar \Gamma}{2 k_B}, \tag{3}$$

where Γ denotes the *natural linewidth* of the atomic transition spectral line, which is determined by the upper-state lifetime τ of the transition $\Gamma = 1/\tau$ [11]. Although the aforementioned T_r and T_D are theoretical temperature limits, several sophisticated laser cooling techniques exist that can achieve even lower temperatures.

2.2.2 Scattering Rate & Power Broadening

An electronic transition for an atom can be approximated using a closed 2-level system, which is only made up of a ground and excited state. By driving the transition with resonant light, atoms will absorb photons and populate the excited state, after which they decay back towards the ground state. This cyclic behaviour is named, a Rabi cycle. The photon absorption rate of an atomic transition in a 2-level system is called the total scattering rate Γ_{SC} and is given by

$$\Gamma_{SC} = \frac{\Gamma}{2} \frac{I/I_{sat}}{1 + I/I_{sat} + 4\Delta^2/\Gamma^2}, \tag{4}$$

where Δ is the laser detuning from the atomic resonance, I is the intensity of the light and I_{sat} is the saturation intensity, which is defined as

$$I_{sat} = \frac{\pi h c}{3\lambda^3 \tau}, \tag{5}$$

where λ is the wavelength and τ is the excited state lifetime [10]. When the light intensity is much greater than the saturation intensity $I \gg I_{sat}$ the total scattering rate saturates to $\Gamma/2$. So this effectively allows larger detuning from resonance, while still addressing the transition. This behaviour is called *power broadening* of the transition linewidth. In practice this effect causes the linewidth of a transition to be broadened from Γ to

$$\Gamma_P = \Gamma \sqrt{1 + I/I_{sat}}, \tag{6}$$

where Γ_P is the power broadened linewidth [10].

2.3 Magneto-Optical Trap

The magneto-optical trap (MOT) is widely used for trapping neutral atoms with the use of both optical and magnetic fields. The trapping of atoms using a MOT was first realised in 1987 by Raab *et al.* for neutral sodium [4]. The working principle of a MOT combines the radiative pressure of light and the Zeeman effect to cool and confine atoms to the trap center.

2.3.1 Magnetic Quadrupole Field

In a MOT a spatially-varying quadrupole magnetic field is created by two coils configured in an anti-Helmholtz configuration, as shown in figure 1. The magnitude of the magnetic field is zero in the center of the quadrupole field and increases with distance from the center. It is important to note that the quadrupole field itself does not necessarily trap neutral atoms. To produce confinement of the atoms the addition of an optical molasses is needed.

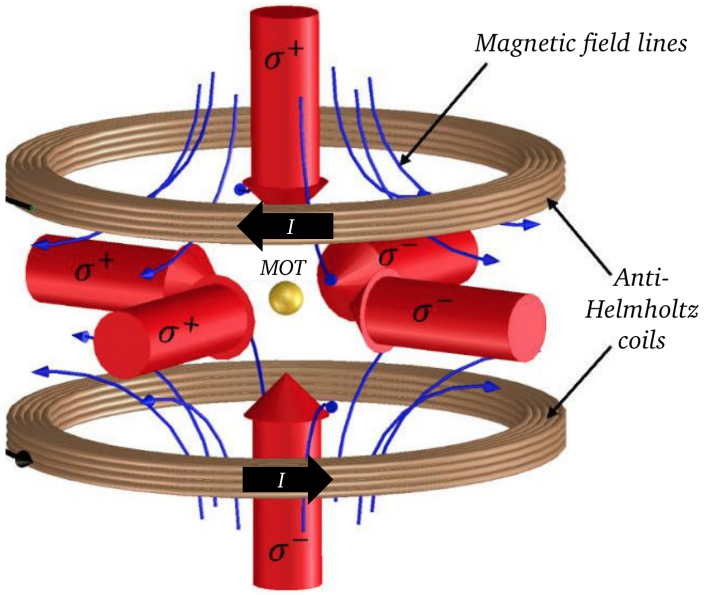


Figure 1: Overview of a 3D MOT. The red-detuned circularly-polarized ($\sigma^{+/-}$) beams are shown as red arrows. The quadrupole field lines are depicted in blue. The direction of current through the anti-Helmholtz configured coils is shown by the black arrows. Original image edited from Mcclelland *et al.* (2015) [12].

2.3.2 Optical Molasses

An optical molasses without the presence of a magnetic field cools down atoms but does not confine them. In this case atoms that move towards a red-detuned beam experience a Doppler shifted beam such that the absorption rate of the counterpropagating beam is increased and that of the opposing beam is decreased. This results in a dissipative force that opposes the motion of the atom. This explains the term *optical molasses*, since atoms are slowed as if they were moving trough viscous substance. To actually trap atoms in the MOT a restoring force, which pushes atoms back towards the center, needs to be present.

2.3.3 Zeeman Effect

To understand how the MOT beams deliver a restoring force to the atoms, consideration of the Zeeman effect is helpful. The Zeeman effect describes the energy shift of atomic states induced by the presence of a magnetic field. The magnitude of the Zeeman shift is given by

$$\Delta E_Z = \mu_B g_J \vec{J} \cdot \vec{B}, \tag{7}$$

where μ_B is the Bohr magneton, g_J is the Landé g-factor and $\vec{J}$ is the total angular momentum. When the quantization axis is chosen to align with the magnetic field $\vec{B}$, the scalar product will reduce to $m_j \cdot |\vec{B}|$, where m_j is the projection of the total angular momentum onto the quantization axis. Since the quadrupole B-field varies spatially, the Zeeman shift will also vary spatially and increase with distance from the center of the trap. The Zeeman shift of an atomic $J = 1$ state in a MOT induced by a spatially-varying B-field is shown in figure 2.

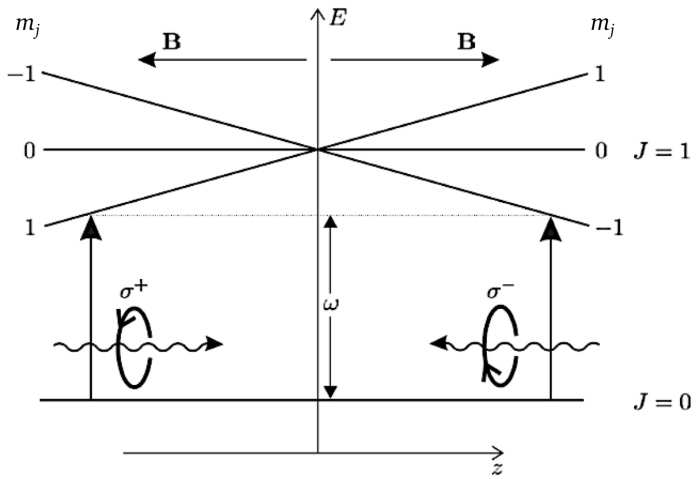


Figure 2: The Zeeman shift of atomic $J = 1$ states in a 1-dimensional MOT brings atoms away from the center in resonance with one of the red-detuned circularly-polarized ($\sigma^{+/-}$) light, pushing the atoms towards the center as a result of the radiative pressure of the light.

Transition	$\Gamma/2\pi$	λ (nm)	T_D	T_r	I_{sat}
$^1S_0$ - $^1P_1$	30.5 MHz	461	730 μK	1.02 μK	40.7 mW/cm^2
$^1S_0$ - $^3P_2$	7.4 kHz	698	180 nK	460 nK	3.0 μW/cm^2
$^3P_2$ - $^3D_2$	2.7 MHz	497	64.8 μK	880 nK	2.9 mW/cm^2

Table 2: Cooling and repumping transition characteristics. Data obtained from PhD thesis by S. Stellmer (2013) [8].

Where in an optical molasses without a magnetic field the absorption rate of red-detuned light is dependent on the velocity of atoms, in a MOT it also depends on the spatial position of the atom. Referencing to figure 2, when an atom moves in the positive z direction it will get in resonance with the σ^- polarized light and be pushed back to the trap center. When the atom moves in the negative z direction it will become resonant with the σ^+ polarized light and once again be pushed towards the trap center.

2.4 Energy Levels and Transitions

2.4.1 Cooling Transitions

Bosonic strontium has two optical cooling transitions that are commonly used, those addressing the $^1P_1$ and $^3P_1$ states from the $^1S_0$ ground state.

The strong transition with broad linewidth $\Gamma \approx 2\pi$ x 30.5 MHz between the $5s^2$ $^1S_0$ ground state and the $5s5p$ $^1P_1$ excited state in strontium is used to cool the atoms down to about a millikelvin T_D = 730 μK. The MOT that operates on this transition has a wavelength of 461 nm which is visible blue light, for this reason we call this the blue MOT transition.

The second cooling transition uses the intercombination line $^1S_0$ - $^3P_1$, which has a wavelength of 689 nm, which is visible red light, for this reason the MOT that operates on this transition is called the red MOT. The red MOT transition has a much narrower linewidth $\Gamma \approx 2\pi$ x 7.4 kHz and can cool the atoms down further to hundreds of nanokelvin T_r = 460 nK and close to quantum degeneracy [8]. Table (2) shows several cooling parameters of the cooling transitions. Both cooling transitions are shown in figure 3.

2.4.2 Leaking into the $^3P_2$ reservoir

During MOT cycles, atoms are continuously transitioning from the ground state to the excited state and back. From the blue MOT cycle $^1S_0$ - $^1P_1$, there is a small decay channel from the $^1P_1$ state into the 5s4d $^1D_2$ state. On average it takes around 50,000 blue MOT cycles for the decay towards 5s4d $^1D_2$ to occur [8]. Because this decay occurs rarely and therefore is relatively slow,

it is often referred to as *leaking* from $^1P_1$ to 5s4d $^1D_2$.

After leaking into the 5s4d $^1D_2$ state, atoms decay further into the $^3P_2$ and $^3P_1$ state, in a 1:2 ratio respectively. Because the $^3P_2$ metastable state is magnetically trappable and long lived, it provides a reservoir of atoms that can be used for many different experiments in atomic quantum physics.

2.4.3 Repumping the $^3P_2$ reservoir

The amount of atoms in the $^3P_2$ reservoir cannot be measured directly, first the atoms need to be transferred back into the ground state, after which the MOT fluorescence or absorption can be measured. Atoms are *repumped* from the $^3P_2$ reservoir, back into the ground state by a repumping laser on the $^3P_2$ - $^3D_2$ transition with $\lambda = 497$ nm and $\Gamma \approx 2.7$ MHz. From the $^3D_2$ state, atoms can decay towards the $^3P_1$ state from which they can return to the $^1S_0$ ground state by the $^1S_0$ - $^3P_1$ red MOT transition. The repumping process is highlighted in figure 3 by the green arrows. While the $^3P_2$ - 5s5d $^3D_2$ repumping transition is used in this experiment, different repumping schemes from the metastable $^3P_2$ state do exist [8].

Figure 3 shows the energy levels and transitions used in the cooling and trapping of strontium. Section 2.5 will introduce the novel approach used in this experiment; the addition of a depumping laser on the $^1P_1$- 5s5d $^1D_2$ transition.

2.5 Depumping towards 5s5d $^1D_2$

Atoms leak into the $^3P_2$ reservoir while the blue MOT is operating. This leaking process is inefficient since it causes long $^3P_2$ loading times for experiments, ~seconds. When numerous experimental cycles are needed, this will hamper the ability to do a lot of measurements in a reasonable time. By increasing the loading rate of atoms into the $^3P_2$ state, the experimental cycle will take less time and be more efficient.

In the hope of improving $^3P_2$ loading rate, a previously unused *depumping* transition is addressed, namely, the 5s5p $^1P_1$ - 5s5d $^1D_2$ transition. This is called depumping, since atoms are *pumped* out of the blue MOT cycle from 5s5p $^1P_1$ towards 5s5d $^1D_2$. To be able to depump on the 5s5p $^1P_1$ - 5s5d $^1D_2$ transition, the precise wavelength or frequency of the transition needs to be known. In a review on wavelengths, transition probabilities and energy levels of neutral strontium, Samsonetti and Nave (2010) refer to an observed wavelength value in a PhD thesis from 1938 by Sullivan of 767.5189(2) nm [13]. Unfortunately, the original source article from

Transition	$\Gamma/2\pi$	λ	I_{sat}
$^1P_1$ - 5s5d $^1D_2$	1.0(4) MHz	767.5189(2) nm	0.30(8) mW/cm^2

Table 3: Depumping transition characteristics. Calculated using wavelength value from Samsonetti and Nave (2010) [13].

Sullivan could not be found. Vaeck *et al.* (1988) give an observed wavelength of 767.524(6) nm and estimate the natural linewidth (Γ) to be $6.6(16)\cdot 10^6$ s^{-1} [14]. Corliss and Bozman (1962) estimate $\Gamma = 6.8(27)\cdot 10^6$ s^{-1} [15]. Using the literature value for the wavelength, the saturation intensity was calculated and is shown in table (3).

No prior experiments were found that documented the decay path from 5s5d $^1D_2$ to $^3P_2$. A diagram of the energy levels and transitions that were used is given in figure 3.

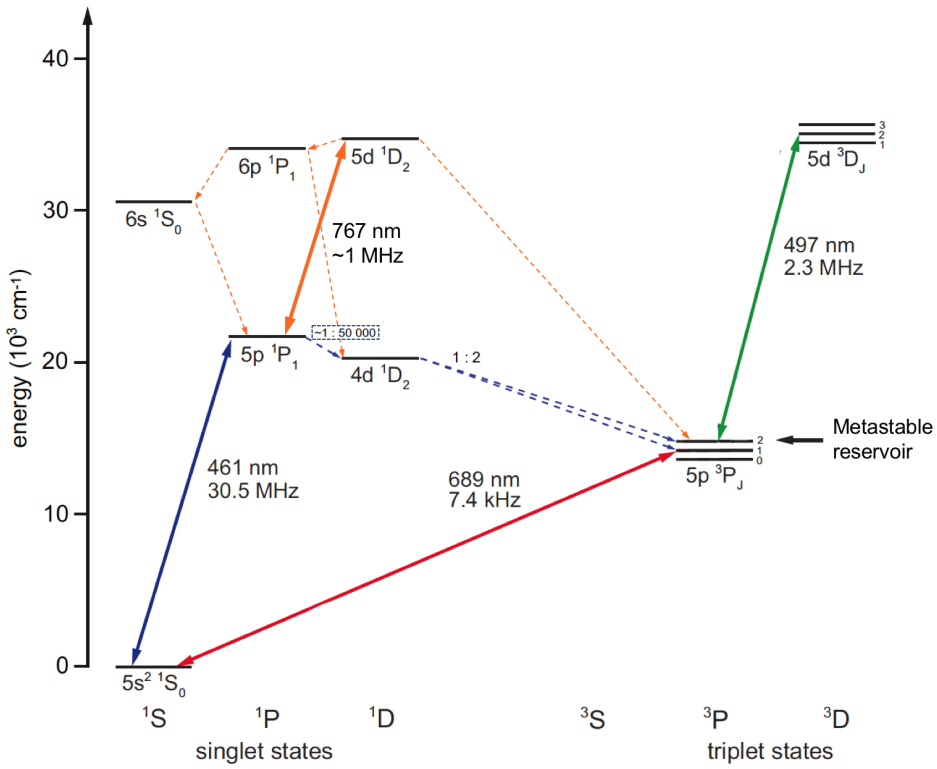


Figure 3: Overview of the energy levels and transitions in strontium. The 767 nm depumping transition from $^1P_1$ towards 5s5d $^1D_2$ is added in orange. Decay transitions are shown as dashed lines. For transitions that were addressed experimentally, λ and $\gamma = \Gamma/2\pi$ are shown. The linewidth of the decay towards from 5s5d $^1D_2$ to $^3P_2$ is unknown. Diagram sourced and edited from PhD thesis by S. Stellmer (2013) [8].

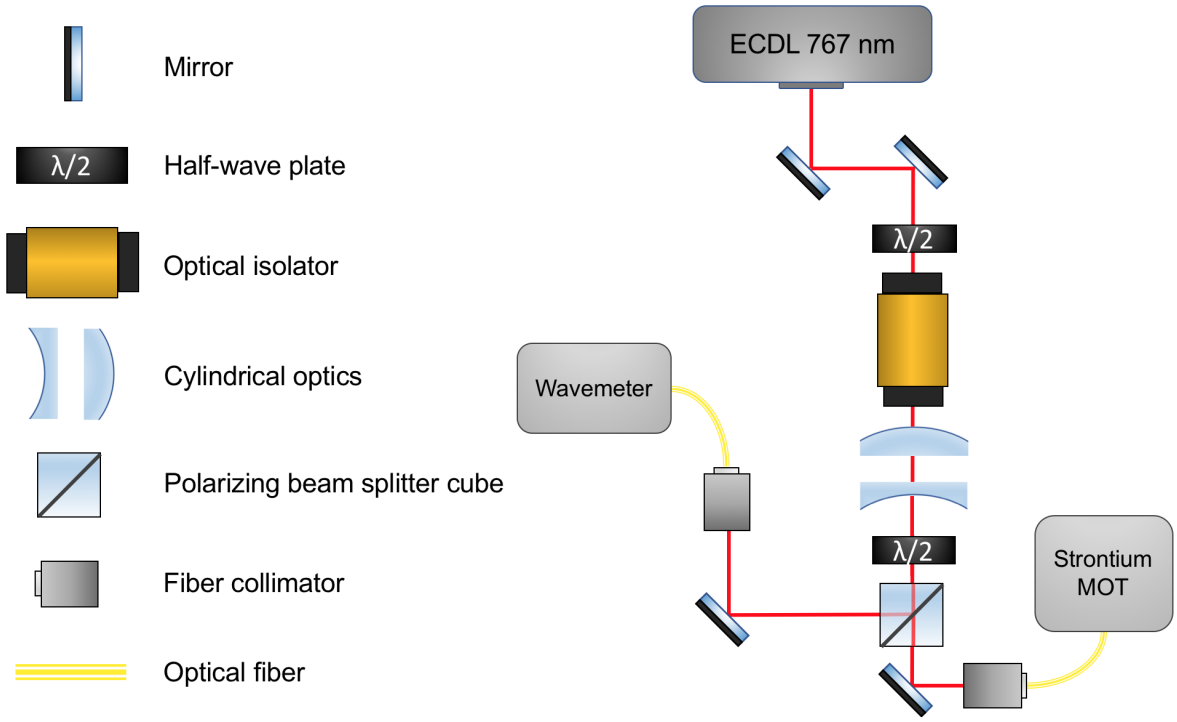


Figure 4: Diagram of the optical setup.

3 Methodology & Setup

This section describes the optical setup that was used to depump the strontium MOT with 767 nm light. A diagram of the complete optical setup is shown in figure 4. To provide better insight in the working of optical setup, the following sections will highlight the components that were used.

3.1 Laser System

To depump atoms in the $^1P_1$ state towards 5s5d $^1D_2$, light is needed with a wavelength of 767.5 nm [13]. A SAL-780-100 laser diode from Sacher Lasertechnik was used for this experiment. The power output of this diode is centered around 780 nm and has a FWHM of ~ 20 nm. To achieve the precise wavelength that was needed for the transition, the ability to fine tune the emitted wavelength by the laser diode is required. This wavelength tunability is made possible by using the laser diode in an external-cavity diode laser setup.

3.1.1 External-Cavity Diode Laser

In an external-cavity diode laser (ECDL) the laser cavity is not enclosed in the laser diode itself, but instead extends outside the diode. The ECDL that was used in this experiment was

set up in the Littrow configuration, in which the laser cavity is formed between the diode and a diffraction grating. The grating can be rotated to adjusts the wavelength and frequency of the output light. Figure 5 provides a schematic representation of an ECDL in Littrow configuration.

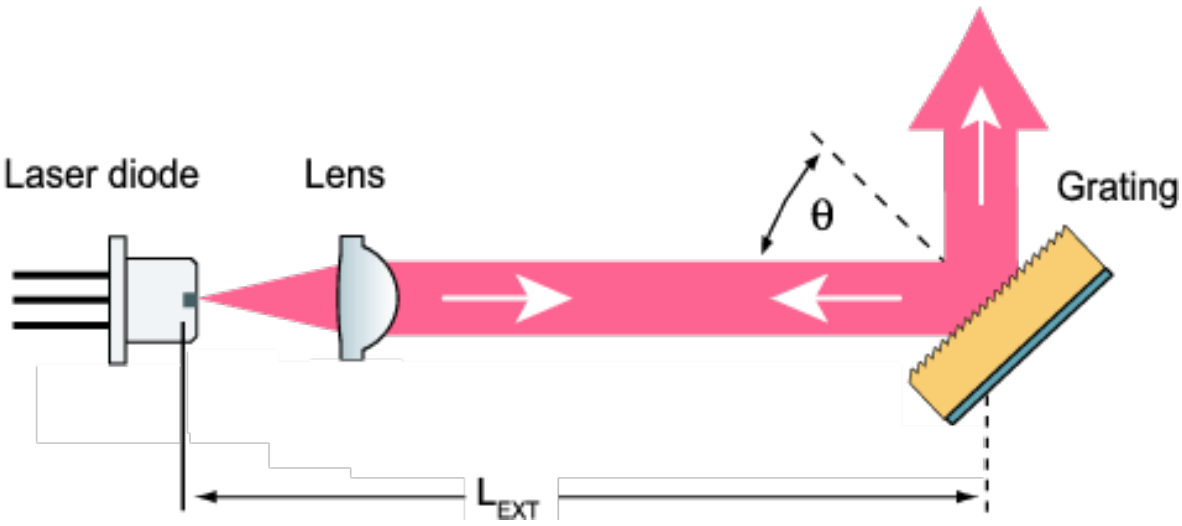


Figure 5: Schematic representation of an ECDL in Littrow configuration. L_{EXT} shows the laser cavity length and θ gives the angle between the normal of the diffraction grating and the incoming beam. Original image edited from Saliba and Scholten (2009) [16].

3.1.2 Wavelength Tuning

In order to measure the wavelength or frequency of the laser, the laser light was sent into a *wavemeter*, made by HighFinesse. To tune the wavelength of the laser, a set screw was used to rotate the diffraction grating to roughly the right wavelength. For fine tuning, a piezoelectric transducer, from now on referred to as the *piezo*, was used to rotate the grating with much more precision. When a voltage is applied over the piezo element, it expands slightly and rotates the grating in doing so. The ECDL with diffraction grating and piezo used in the experiment are shown in figure 6.

3.1.3 Laser Characteristics

The laser was constructed in 2014 by Meinster (MSc) to rebuild a MOT system used for potassium-40, that was part of Prof. Dr. Jook Walraven's quantum gas research group between 2004 and 2012 [17]. The minimum current required for the laser to start lasing, called the threshold current, was measured to be ~55 mA at 767 nm in 2014. On 26/06/2016 the diode was documented to have a lasing threshold current of ~150 mA at 767 nm [18]. This shows that the

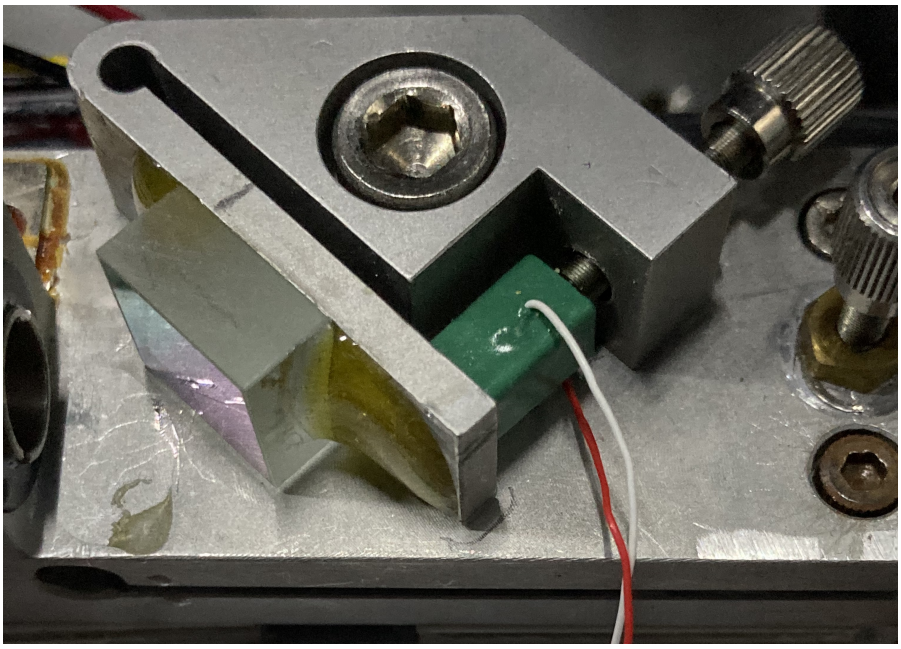


Figure 6: Image of the ECDL. The diffraction grating can be rotated using the set screw in the top right or with the (green) piezo element.

performance of the diode has worsened since it was taken in operation.

To see if the condition of the diode has decreased further since it was used in 2016, the laser output power was measured as a function of input current and is shown in figure 7. The threshold current for 780 nm is 80 mA, for 767 nm it is 150 mA, the same as it was in 2016. In table (4) some laser characteristics that were important for this experiment, are summarised.

The wavelength or frequency of the laser is not perfectly stable: when the temperature of the laser fluctuates, the wavelength does as well. This is due to a change in laser cavity length caused by thermal expansion of the laser cavity in the ECDL. To limit temperature fluctuations of the laser, a Peltier element that is controlled with a PID, stabilises the temperature. In the experiment, a cardboard box was placed over the ECDL housing to protect it from air flow and provide further thermal insulation.

The rectangular geometry of the laser diode causes the beam shape to be elliptical instead of circular. Section 3.4 will contain a more detailed look at the elliptical beam shape and introduce the corrective optics used in the experiment.

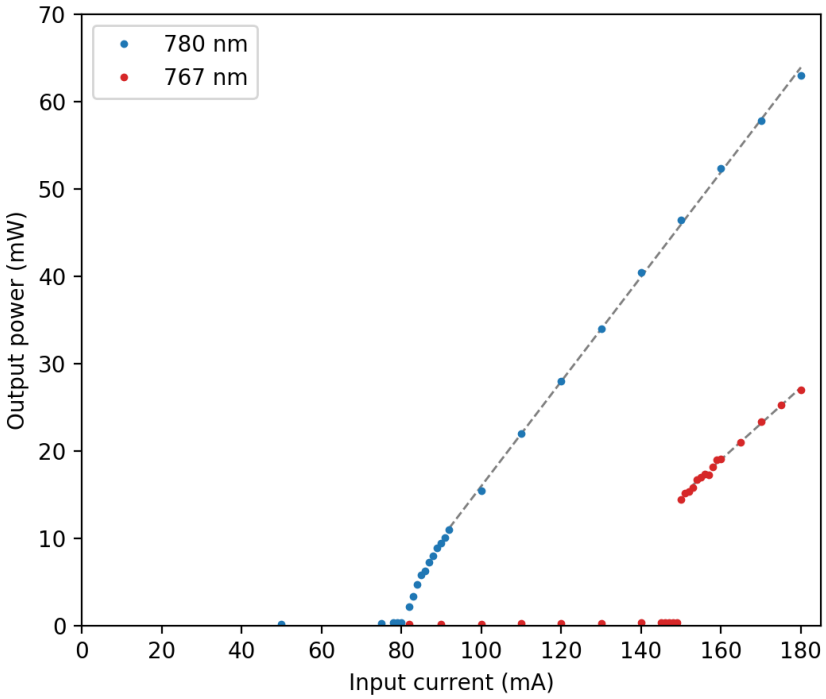


Figure 7: The laser output power plotted against the input current. The threshold current for 780 nm is ~80 mA and for 767 nm it is ~150 mA. Error in power measurement is smaller than symbol size. Fit lines show the linear relation between input current and output power.

Laser diode max. current	185 mA
Laser diode operating current	~170 mA
Operating output power	25 mW
Operating temperature	19.3 °C
Piezo voltage range	0 - 100 V

Table 4: Laser characteristics. Includes operating values used in the experiment.

3.2 Optical Isolator

An optical isolator (IOT-5D-767-VLP) is placed in the optical setup to protect the laser from backwards propagating light that travels back into the laser cavity, since optical feedback can cause instability in the lasing frequency. First the optical isolator is configured to maximize beam attenuation by placing it in reverse orientation in the optical setup. Afterwards the isolator is flipped back to its correct orientation. To characterise the transmission of light through the isolator, the relative transmission is measured as a function of polarisation angle and is shown in figure 8. The polarisation angle of the incoming light was altered using a half-wave plate, the transmitted power was measured using a Thorlabs power meter. The maximum transmission of the isolator was measured to be ~70 % with an attenuation of ~40 dB. The fitted sine curve does not pass through all data points, this is likely due to fluctuations in laser intensity.

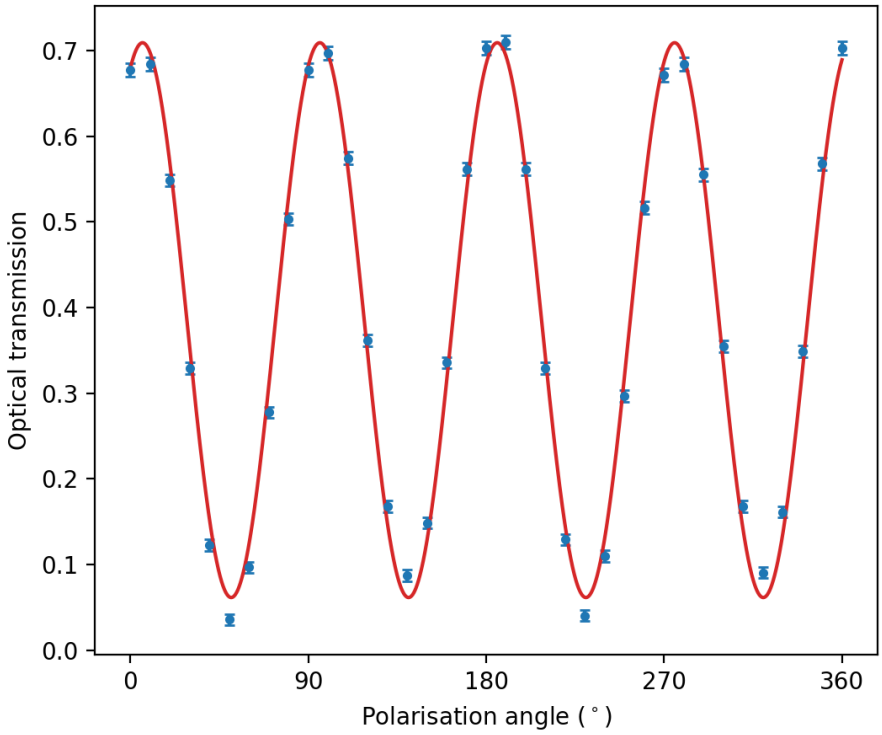


Figure 8: Light transmission through the optical isolator for different polarisation angles. A fitted sine curve through the measurements is shown in red. The polarisation angle is altered using a half-wave plate. The error bars show the uncertainty in transmission due to precision in power measurement readings. the amount of power measured before and after the isolator. Optical isolator: IOT-5D-767-VLP by Optics for Research.

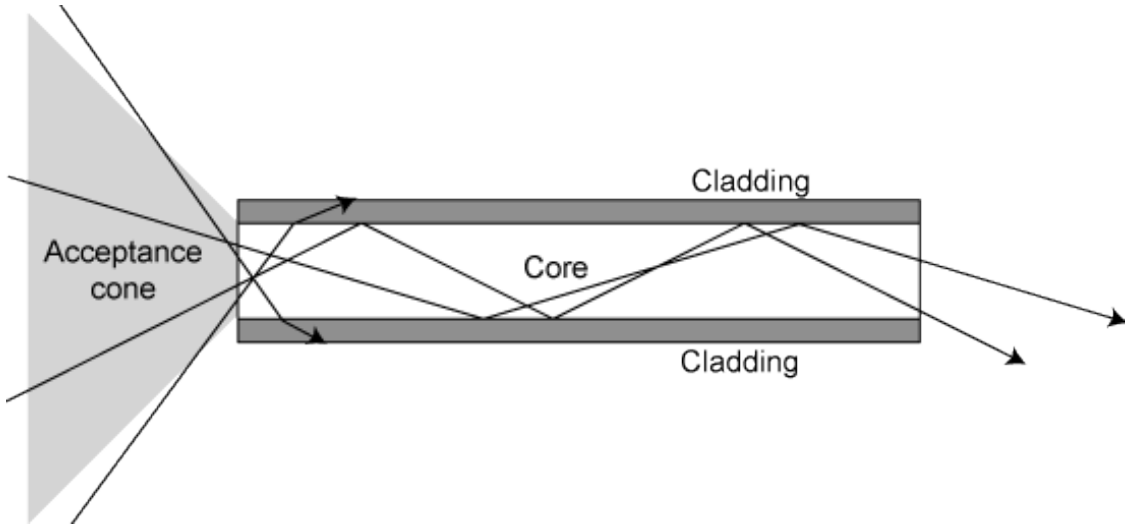


Figure 9: Illustration of an optical fiber. Light that is outside the cone of acceptance, will not be transmitted through the fiber.

3.3 Optical Fibers & Collimators

The laser light is transported from the optical setup to the strontium atoms inside the MOT, using an optical fiber. Figure 9 contains an illustration of the internal part of an optical fiber. Light is able to travel through the fiber due to total internal reflection inside the fiber core. Total internal reflection occurs on the core-cladding interface when the angle of incidence of the incoming light is greater than the critical angle $\theta_{in} > \theta_{crit}$, with θ_{crit} given by

$$\theta_{crit} = \sin^{-1}\left(\frac{n_{clad}}{n_{core}}\right), \tag{8}$$

where $n_{clad,core}$ gives the index of refraction of the cladding and core respectively [19]. With Snell's law, the acceptance angle (θ_{max}) can be defined as

$$\theta_{max} = \sin^{-1}\left(\frac{1}{n_0}\sqrt{n_{core}^2 - n_{clad}^2}\right), \tag{9}$$

where n_0 gives the index of refraction of the medium outside the fiber [19]. The *numerical aperture* (NA) is defined as $n_0 \sin\theta_{max}$. The square of the NA is a measure of the light-gathering power of an optical fiber. In this case the fibers are used in air, which has refractive index $n_0 \approx 1$, so the NA for the fibers is given by

$$\text{NA} = \sqrt{n_{core}^2 - n_{clad}^2}. \tag{10}$$

The optical fibers used in this experiment are from Thorlabs and have a cutoff wavelength under 767 nm. The used fibers are *single mode*, this means that the fibers will only transmit light in a Gaussian *fundamental* mode; the TEM_{00} mode, where TEM stands for *transverse*

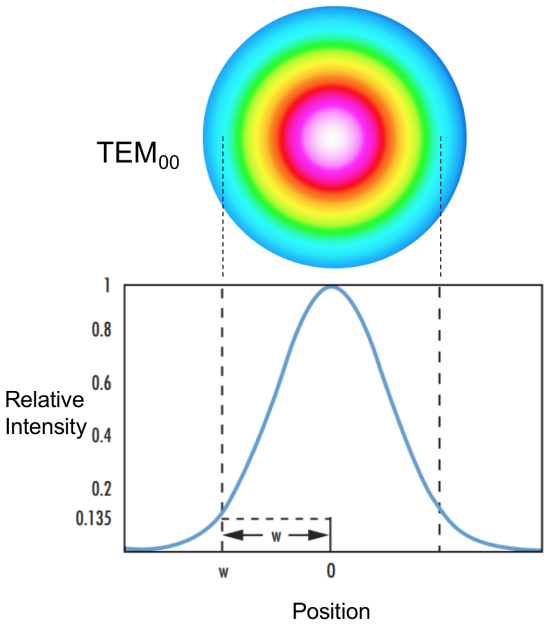


Figure 10: The Gaussian fundamental TEM_{00} mode with intensity distribution. w depicts the waist of the beam; the radius at which the intensity has fallen to $1/e^2 \approx 0.135$ of the intensity at the center.

electromagnetic. This mode has a circular beam shape with a Gaussian intensity distribution, as is shown in figure 10. To efficiently transmit light through the single mode fiber, the light needs to be in this mode before it is injected into the fiber.

The actual core of the optical fiber is only a few μm's in diameter, so the laser light also needs to be focused on this core. This is done with a fiber collimating lens. The NA of the fiber and the focal length f of the collimating lens define the beam diameter for injecting into the fiber. The beam diameter $Ø_{beam}$ that will be accepted into an optical fiber is given by

$$Ø_{beam} = 2 \cdot f \cdot \mathrm{NA} \cdot 0.82, \tag{11}$$

where 0.82 is a correction factor to account for differences in definition. The fiber collimating lenses that were used in the optical setup are from Thorlabs.

3.4 Optimising Beam Shape

The laser produces an elliptical beam shape, caused by the geometry of the laser diode. The beam shape needs to be adjusted to inject light into the optical fiber more efficiently.

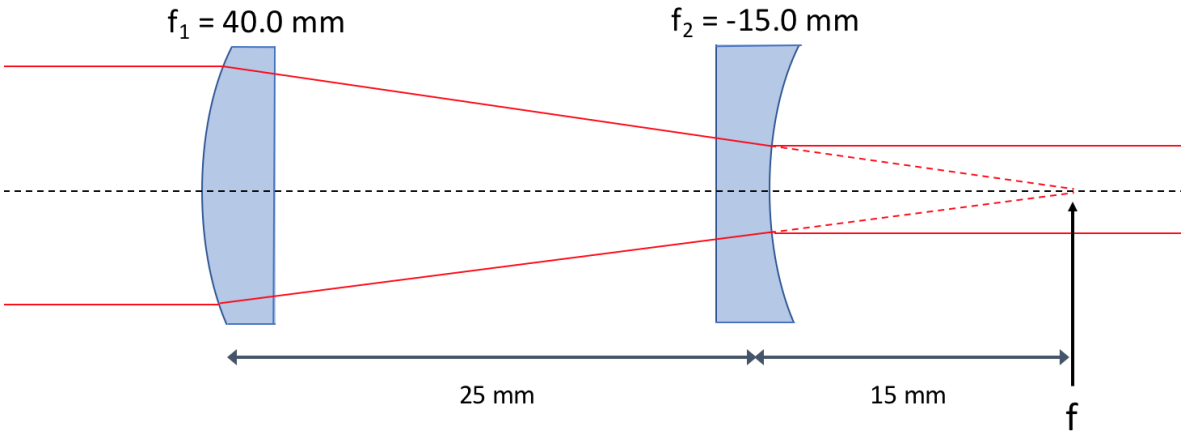


Figure 11: Cylindrical Galilean telescope used for adjusting the beam shape. The convex lens on the left has focal length f_1 = 40.0 mm and the concave lens has negative focal length f_2 = −15.0 mm. The telescope has a magnification factor of M =f_2/f_1 = 0.375

3.4.1 Beam Waist & Intensity Distribution

To measure the beam shape a UI-3240ML camera from IDS was used, which has a matrix size of 1280 x 1024 pixels with a pixel size of 5.30 µm. Figure 12a shows the elliptical beam shape that is emitted by the laser. To determine the beam waist, the intensity profile was fitted to a 2-dimensional Gaussian given by

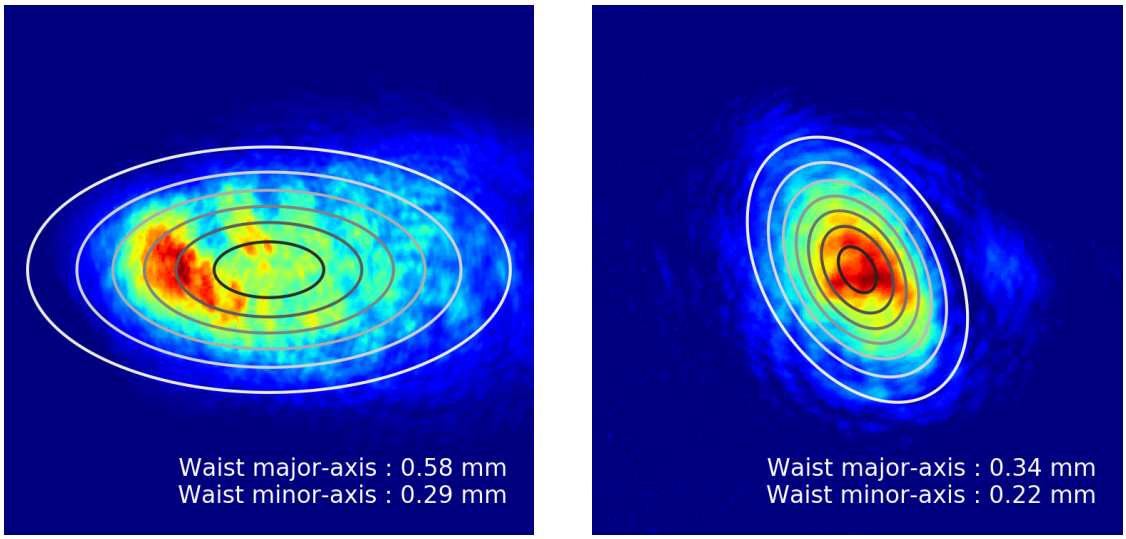
$$f(x,y) = A \cdot e^{-\frac{2(x-x_0)^2}{w_x^2}} \cdot e^{-\frac{2(y-y_0)^2}{w_y^2}}, \tag{12}$$

Where A gives the maximum intensity of the Gaussian and $w_{x,y}$ gives the beam waist of both the axes. Using this 2D Gaussian fit, the major-axis beam waist was estimated: w_{major} =0.58(5) mm and the minor-axis beam waist: w_{minor} =0.29(5) mm. To reshape the beam to be more circular, the major-axis of the ellipse needs to be reduced while leaving the minor-axis intact.

3.4.2 Cylindrical Optics

A spherical lens focuses all the incoming light into a single point, while a cylindrical lens focuses the light onto a line. Rephrased, a cylindrical lens only focuses one axis of incoming light, instead of two. This makes it possible to focus the major-axis of the ellipse, making the beam shape more circular in the process. Figure 11 shows a diagram of the cylindrical Galilean telescope that was used to adjust the beam shape.

The cylindrical Galilean telescope uses a plano-convex and plano-concave mirror with focal lengths of 40.0 mm and -15.0 mm respectively. Using a concave mirror keeps the total length



(a) Without cylindrical optics

(b) With cylindrical optics

Figure 12: Beam intensity profiles with 2D Gaussian fit. (a) Elliptical beam shape from the laser diode. (b) Beam shape adjusted with cylindrical optics.

of the telescope small, since this is given by the sum of focal lengths. The magnification of the telescope is given by the ratio $M = |f_2/f_1| = 15/40 = 0.375$.

The beam shape after passing through the cylindrical optics is shown in figure 12b. The major-axis is 0.34(5) mm and the minor axis is 0.22(5) mm. To check if the beam size is sufficiently small to pass through the fiber, equation (11) is used to calculate the maximal beam diameter that is accepted by the optical fiber $Ø_{max} = 0.81$ mm. The maximal beam diameter of the laser light is double the major-axis waist $Ø = 0.34 * 2$ mm $= 0.68$ mm. So the beam is indeed small enough to be injected into the optical fiber. The beam is not perfectly circular after the cylindrical telescope, the major axis of the original beam seems to have been shrinked down too much. This indicates that the magnification factor of the telescope was too small. Furthermore, the beam intensity distribution seems to be rotated compared to the original beam shape, which could mean that the cylindrical telescope was not properly aligned with the major-axis of the original beam. Nevertheless, the observed transmission efficiency through the fiber was 65%, which was sufficient for this experiment.

After the laser beam has passed through the cylindrical optics and is ready to be coupled into an optical fiber, a polarizing beam splitter (PBS) cube splits the beam into two different optical paths, as shown in figure 4. The polarisation of the light is altered using a half-wave plate in such a way that the PBS cube splits the light in a low and high intensity path. The low

intensity light is sent to the wavemeter from HighFinesse, to determine the frequency of the light. The high intensity beam is sent towards the atoms inside the MOT chamber. To measure the effect that the 767 nm depumping light has on the atoms inside the MOT, two methods were used: measuring fluorescence and absorption by atoms inside the MOT.

4 Results

4.1 Blue MOT Fluorescence

When the $^1P_1$ state is depumped toward 5s5d $^1D_2$, atoms are no longer in resonance with the blue MOT light and are lost from the blue MOT cycle, thus decreasing the fluorescence from the blue MOT. This decrease in fluorescence was measured using a Thorlabs power meter.

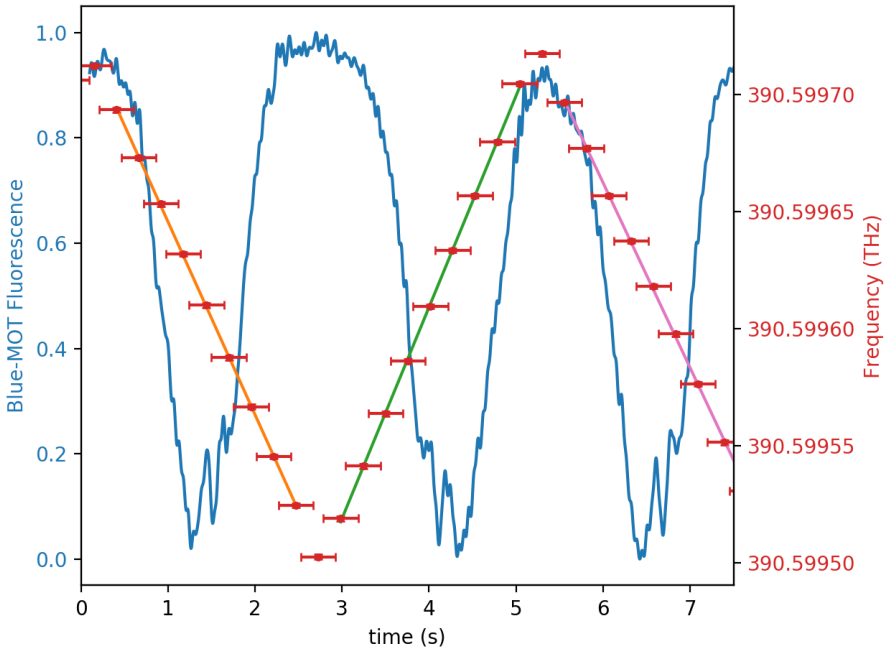


Figure 13: Blue MOT fluorescence signal during a frequency sweep of the 767 nm depumping laser. A low-pass filter (< 20 Hz) was used on the blue MOT fluorescence signal to reduce signal noise. The fluorescence signal has been rescaled using min-max normalization. Linear fits were made of the frequency sweeps and are shown in orange, green and pink. Error bars indicate the uncertainty in time as a result of overlapping the data by eye of 0.2 s.

By performing a frequency sweep with the depumping laser near the frequency corresponding to the transition, a decrease in blue MOT fluorescence was measured. Figure 13 shows the blue MOT fluorescence signal (blue line) during a frequency sweep of the depumping laser, as

measured on the wavemeter (red line). The intensity of the depumping beam was I = 0.9(3) mW / cm^2 $\approx 3I_{sat}$. Using fast Fourier transform (FFT) a low-pass filter was applied for frequencies over 20 Hz, to reduce noise on the fluorescence signal. The fluorescence signal was rescaled using min-max normalization. The fluorescence signal data and frequency data are overlapped by eye using the signal peaks and dips as reference, which leads to uncertainty in time as shown by the error bars. Linear fits were made of the frequency sweeps to be able to map the blue MOT fluorescence data to the depumping frequency data. The linear fits have an average slope of 85 ± 5 MHz/s where 5 MHz/s is the standard deviation of the slopes.

The blue MOT fluorescence as a function of depumping frequency is shown in figure 14. Measured with a depumping intensity of $I \approx 3I_{sat}$. The orange, green and pink data correspond to the linear fits of frequency sweeps of figure 13. The dip in blue MOT fluorescence was fitted to a Lorentzian, which was centered at 390.59962(2) THz.

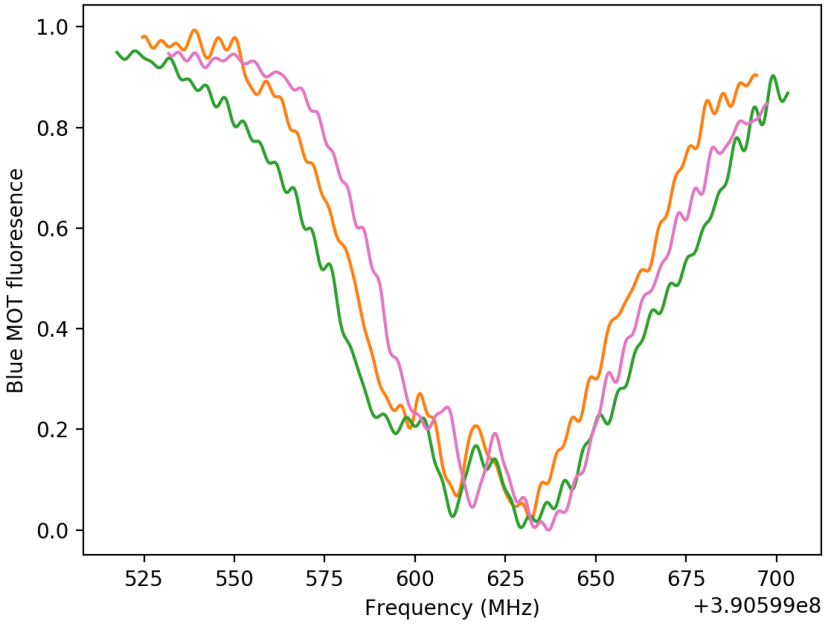


Figure 14: The blue MOT fluorescence as a function of depumping laser frequency. The orange, green and pink data correspond to the linear fits of figure 13. Lorentzian fits were made on the data with an average FWHM of 56 MHz, centered at 390.59962(2) THz. The uncertainty in frequency of 20 MHz is calculated using the the linear fit slope (85(5) MHz/s) and uncertainty in time due to overlapping data (0.2 s).

4.2 Atom Number Enhancement

To measure the effect that depumping has on the amount of atoms in the $^3P_2$ reservoir, atoms are recaptured by the red MOT after repumping them out of $^3P_2$. With the atoms in the red MOT cycle, absorption imaging is used to measure the number of atoms in the MOT.

When resonant light passes through an atomic cloud, the intensity of the passing light will be reduced. The optical density (OD) of the cloud is calculated using the ratio of the light intensity before and after the atomic cloud: $OD = -\ln I/I_0$. Using the optical density, the amount of atoms in the atomic cloud is calculated. Furthermore, absorption imaging provides the possibility to take *time of flight* (TOF) measurements, in which the atomic cloud expands before taking the absorption measurement, which produces a less saturated image.

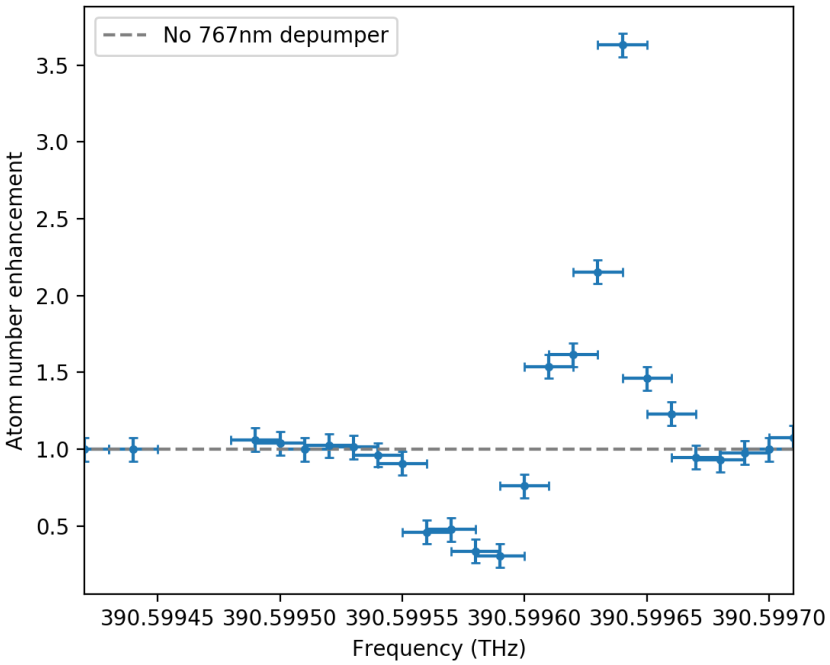


Figure 15: The atom number enhancement is plotted against the depumping laser frequency. A peak in atom number is visible at a frequency of 390.59964(1) THz. Horizontal error bars indicate the uncertainty in frequency of ±10 MHz, since the laser frequency was stabilized by hand within this range. Vertical error bars indicates the precision of the atom number measurement read out.

In figure 15 the atom number enhancement is plotted against the depumping laser frequency. A dip in atom number is visible in the range 390.59955(1) - 390.59961(1) THz while an increase is visible between 390.59961(1) - 390.59966(1) THz. The maximal atom number enhancement

was measured at a frequency of 390.59964(1) THz, with a measured atom number enhancement by a factor of 4.0(3). The atom number without depumping was determined at 1.18(5) $\cdot 10^6$ atoms. The atom number is decreased at 390.59958(1) THz to 0.37(3) times the atom number without depumping. For all atom number measurement the laser frequency was stabilized by hand during the measurements within 10 MHz by adjusting the piezo voltage and simultaneously measuring laser frequency changes with 1 MHz precision.

4.3 Optimal Depumping Intensity

In figure 16 the atom number is plotted against the depump laser saturation $s_{767} = I/I_{sat}$ with $I_{sat} = 0.30(8)\text{mW/cm}^2$. Measurements were done at depumping frequency of 390.59964(1) THz. The peak in atom number enhancement with a factor of 4.6(2) was measured around $I = 0.9(3)\text{mW / cm}^2 \approx 3I_{sat}$.

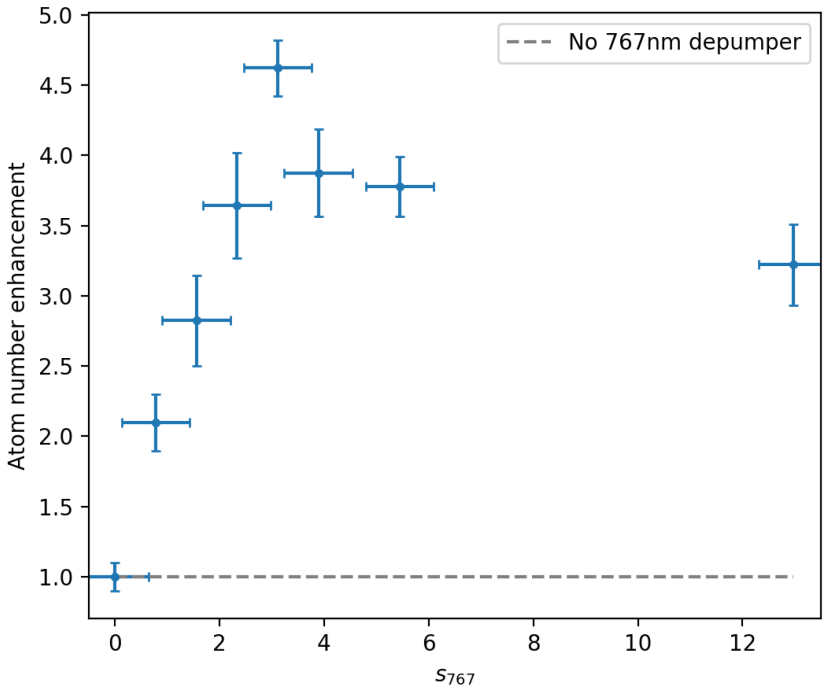


Figure 16: The atom number plotted against the saturation ratio $s_{767} = I/I_{sat}$ with $I_{sat} = 0.30(8)\text{mW/cm}^2$. Measurements were performed 5 or 6 times at a depumping frequency of 390.59964(1) THz and 300 ms loading time. Observed peak in atom number by factor 4.6(2) at $I = 0.9(3)\text{mW / cm}^2 \approx 3I_{sat}$. Horizontal error bars indicate the uncertainty in laser intensity. Vertical error bars are the standard deviation of the mean of the atom number measurements.

4.4 Loading Time Enhancement

In figure 17 the atom number is plotted against the reservoir loading time, with and without the depumping 767 nm laser. Both with and without the 767 nm light the atom number seems to increase linearly with loading time. The slope of the linear fit is equal to the loading rate. The slope of the linear fit without depumping is $1.0 \cdot 10^6$ atoms per second. The slope of the linear fit with depumping is $3.6 \cdot 10^6$ atoms per second.

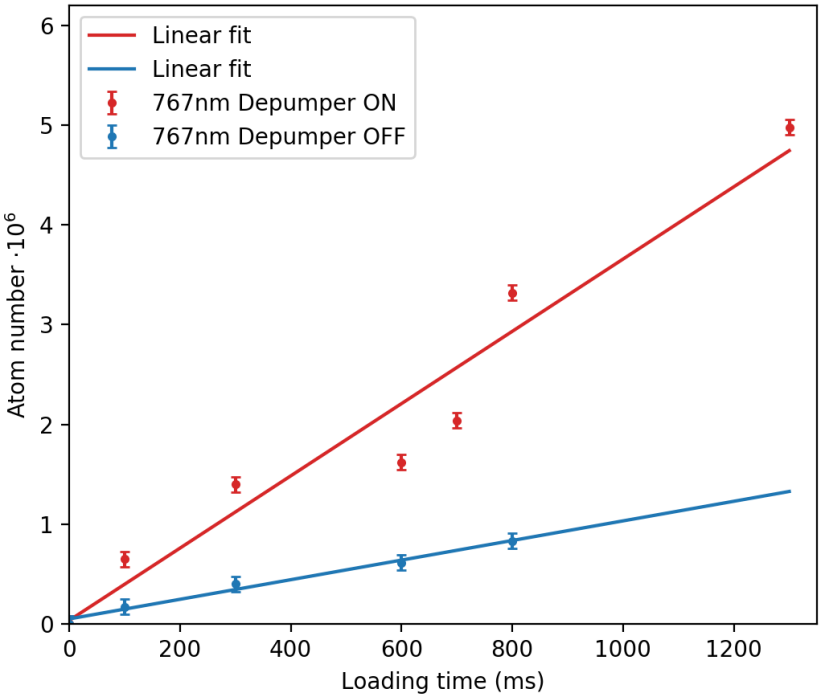
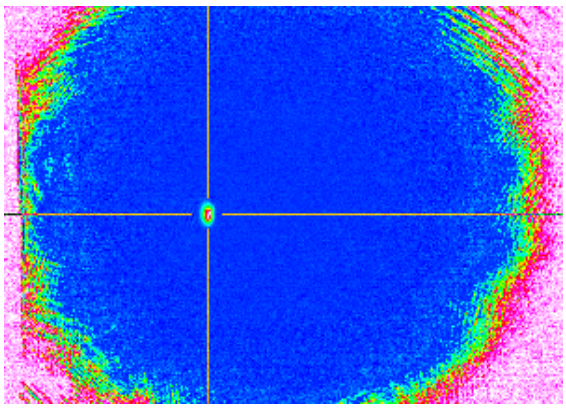
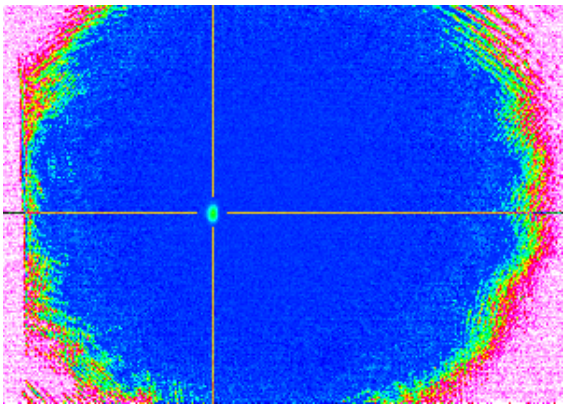


Figure 17: The atom number as a function of reservoir loading time. With the 767 nm depumping laser on, a clear increase in atom number is visible for the same loading time. A linear fit was made through the data points. Measurements were performed at a depumping frequency of 390.59964(1) THz. Vertical error bars shows the atom number measurement precision of 0.1 $\cdot 10^6$ atoms.

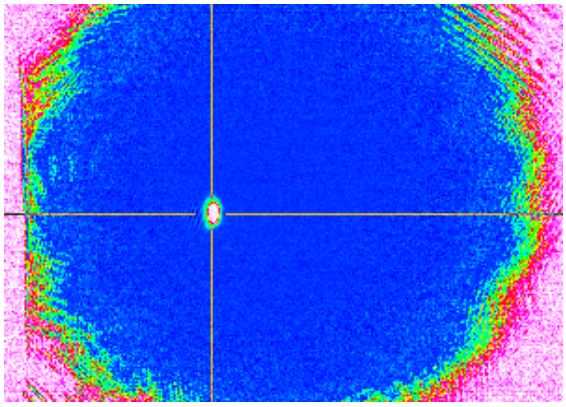
Figure 18 highlights some of the absorption images that were taken to measure the atom number. For an accurate reading of the atom number when depumping at 390.59964(1) THz, a time of flight image needed to be taken since the atom number increase caused the image to be saturated. When allowing an expansion time of 15 ms the atom number increased to 370% compared to no depumping.



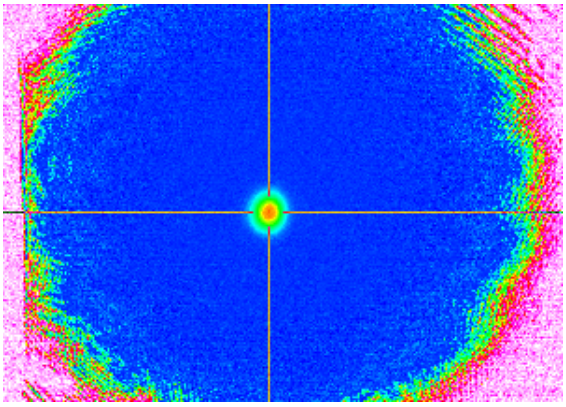
(a) No 767 nm depumping.



(b) Depumping at 390.59958 THz



(c) Depumping at 390.59964 THz (In Situ)



(d) Depumping at 390.59964 THz (15 ms TOF)

Figure 18: MOT absorption images in the case of: (a) No depumping: $1.4 \cdot 10^6$ atoms (b) depumping at 390.59958 THz: $3.7 \cdot 10^5$ atoms (c) depumping at 390.59964 THz: overexposing the image. (d) 15 ms time of flight image with depumping at 390.59964 THz: $5.2 \cdot 10^6$ atoms.

5 Discussion

5.1 Transition Frequency

The MOT fluorescence and absorption measurements show that the light frequency of the $^1P_1$ - 5s5d $^1D_2$ transition is centered around 390.59962(2) THz. This value is inconsistent with the value provided by Samsonetti and Nave (2010) 390.5994(1) THz [13] and is just inside the uncertainty of Vaeck *et al.* 390.597(3) THz [14]. The original source for the value from Samsonetti and Nave is dated 1938 and unfortunately, its experimental methods could not be studied since it was not found online during the literature research of this project. The overlapping of the blue MOT fluorescence data and frequency data was estimated with a uncertainty of 0.2 seconds, this made it impossible to determine the transition frequency more precisely.

5.2 Atom Number Enhancement

In figure 15 the atom number enhancement is shown as a function of the depumping laser frequency. When the laser is red detuned up to 60 MHz from the center of the transition, meaning its frequency is lower than 390.59962 THz, the atom number decreases. If the laser is blue detuned by up to 40 MHz with a frequency larger than 390.59962 THz, the atom number increases. Because the laser frequency was stabilized by hand within 10 MHz, the increase in atom number could not be determined very precisely. During this project there were not a lot of opportunities to gather data to average out laser frequency fluctuations with statistics. For future research it would be advisable to lock the laser frequency, to determine the atom number enhancement with more precision.

A possible explanation for this asymmetric atom number dependence on depumping frequency comes from the fact that only the $m_j = 2,1$ states of $^3P_2$ are magnetically trappable Zeeman states. Only $m_j = 2,1$ are low-field seeking states which are confined by the quadrupole field. A single photon transition can only change the angular momentum with $\Delta J, \Delta m_j = \pm 1, 0$, which means that only the $m_j = 2,1,0$ states of 5s5d $^1D_2$ can directly decay towards the trappable $^3P_2$ states. When the depumping laser preferentially excites atoms to the $m_j = 2,1,0$ Zeeman states of 5s5d $^1D_2$, the decay into the magnetically trappable $m_j = 2,1$ $^3P_2$ states will increase. Figure 19 shows the possible photon transitions towards the $m_j = 2,1,0$ Zeeman states of 5s5d $^1D_2$.

The energy shift of the individual Zeeman states is given by equation (7), since the Landé g-factor of both $^1P_1$ and 5s5d $^1D_2$ is $g_J = 1$, the states will all shift with $\Delta E_Z = \mu_B m_j B$. The three σ^+ transitions are blue detuned by $\Delta E_Z = +\mu_B B$ and the σ^- transitions are red detuned

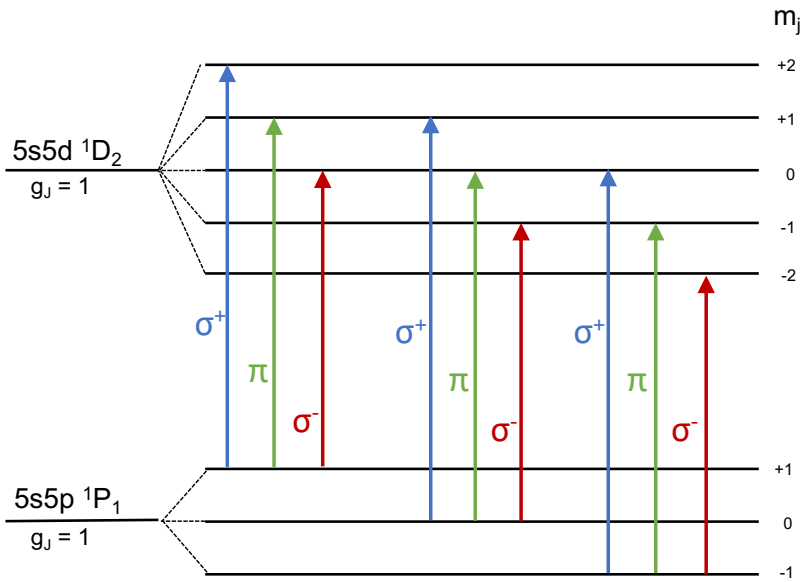


Figure 19: Diagram of Zeeman shifted transition between $^1P_1$ and 5s5d $^1D_2$. The $\sigma^{\pm}$ arrow corresponds to a $\Delta m_j = \pm 1$ transition and the π arrow corresponds to $\Delta m_j = 0$ transition. Both states have a Landé g-factor of $g_J = 1$.

by $\Delta E_Z = -\mu_B B$. The direct decay towards the trappable $m_j = 2,1$ $^3P_2$ states is far more probable after a blue detuned transition, since the atoms will always end up in a $m_j = 2,1,0$ $^1D_2$ state. A red detuned transition will always end up in a $m_j = -2,-1,0$ $^1D_2$ state, from which only the $m_j = 0$ could potentially reach a trappable $m_j = 1$ $^3P_2$ state.

To argue for this explanation, the expected shift in light frequency corresponding to the Zeeman shift of the blue detuned transitions is calculated with

$$\Delta E_{photon} = h \cdot \Delta f \stackrel{!}{=} \Delta E_{Zeeman} = \mu_B B \tag{13}$$

$$\Delta f \stackrel{!}{=} \frac{\mu_B B}{h}, \tag{14}$$

where magnetic field magnitude B of the blue MOT is 55 Gauss / cm, so the expected shift in light frequency is $\Delta f \approx 77$ MHz / cm. In figure 15 the atom enhancement extrema are ~ 40 MHz from the center. So in this case atoms are excited by the blue detuned σ^+ transitions at ~ 0.5 cm from the quadrupole field center.

This positional dependence was also observed in the lab during a frequency sweep: the blue MOT fluorescence was observed while the frequency sweep was performed, which resulted in a temporarily radial darkening from the center that travelled over the image like a radial wave would do on water.

To make this theory more credible, the decay path towards $^3P_2$ could be established more rigorously in further research. Photons that are emitted from the decay from 5s5d $^1D_2$ to $^3P_2$ have an energy corresponding to the energy difference of the transition, one could measure if photons with that specific energy are emitted during the loading of $^3P_2$.

5.3 Loading Time Enhancement

The atom number as a function of loading time is expected to follow $N(t) = N_{max}(1-e^{-\alpha t})$, with N_{max} the maximum saturated atom number and α the loading rate constant. In figure 17 the observed trend seems linear. However, on a short timescale this function is close to being linear. This could mean that the reservoir loading was not saturated yet after 1.3 s. Data that includes longer loading times is needed to show that the increase in atom number decays exponentially with loading time. The slope of the linear fit lines indicate an improvement in loading rate by a factor of 3.6 for loading times up to 1.3 s. To determine the loading rate enhancement accurately, more data points are needed that include longer loading times.

6 Conclusion & Outlook

In summary, in this project a MOT with ^{88}Sr atoms was depumped on the 5s5p $^1P_1$ - 5s5d $^1D_2$ transition. This was achieved by creating a depumping setup from which light was sent into the MOT chamber. By measuring the blue MOT fluorescence during a frequency sweep of the depump laser, the transition frequency of 5s5p $^1P_1$ - 5s5d $^1D_2$ was determined to be 390.59962(2) THz.

To determine the number of atoms in the MOT, absorption imaging was used. The effect of depumping on the atom number was studied. Light that was blue detuned at 390.59964(1) THz, increased the atom number by a factor of 4.0(3). When the light was red detuned at 390.59958(1) THz, the atom number decreases to 0.37(3) times the atom number without depumping.

The optimal depumping light intensity that produced the maximal atom number enhancement by a factor of 4.6(2), was measured at an intensity of 0.9(3) mW / cm^2 = 3(1) I_{sat}. An enhancement in loading rate was observed with depumping. The atom number was measured for loading times up to 1.3 s. The slope of the atom number as a function of loading time is equal to the loading rate, which was estimated using a linear curve fit, was enhanced to a factor of 3.6

The $^3P_2$ loading enhancement offers an exciting prospect, especially for ^{84}Sr, since it has a low natural abundance and as a result loading times form an even bigger part of the experimental cycle. Future research should try to verify that the direct decay from 5s5d $^1D_2$ to $^3P_2$ is used to load atoms into $^3P_2$. To improve the precision of atom number enhancement, a depumping laser with improved frequency stability should be used, by for instance, locking the laser. In addition, the observed atom number increase/decrease for blue/red detuned light, as shown in figure 15, could be compared to a simulation.

Acknowledgements

I would like to thank everyone that was involved in making this bachelor project possible. In the first place, many thanks to Florian, for offering me the possibility to do this project in the strontium quantum gas group. This was not evident since the project consisted primarily out of physical work in the lab during the COVID-19 pandemic. A special thanks to my official and unofficial daily supervisors Ivo & Benjamin, who offered a wealth of knowledge on the subject and helped me in the lab, day in, day out. I would also like to thank Alex, for helping me take measurements and for stabilizing the laser by hand during the measurements. I would also like to encourage Rodrigo to pursue a career in singing, because of his famous rendition of "Can't Help Falling In Love" by Elvis Presley, which is still stuck in my head. Huge thanks to Klaasjan for being my second supervisor on such short notice.

References

[1] R. Frisch, Experimenteller nachweis des einsteinschen strahlungsrückstoßes, *Zeitschrift für Physik* **86**, 42 (1933).

[2] D. Wineland H. Dehmelt, Proposed 1014$\delta\nu/\nu$ laser fluorescence spectroscopy on tl+ mono-ion oscillator iii (side band cooling), *Bull. Am. Phys. Soc* **20**, 637 (1975).

[3] T. W. Hansch A. L. Schawlow, Cooling of gases by laser radiation, *Optics Communications* **13**, 68 (1975).

[4] E. L. Raab, M. Prentiss, A. Cable, S. Chu D. E. Pritchard, Trapping of neutral sodium atoms with radiation pressure, *Phys. Rev. Lett.* **59**, 2631 (1987).

[5] Information for the public. nobelprize.org. nobel prize outreach ab 2021, <https://www.nobelprize.org/prizes/physics/2001/popular-information/>. Accessed: 14-07-2021.

[6] Strontium quantum gas group, van der waals-zeeman institute, university of amsterdam, <http://www.strontiumbec.com/>. Accessed: 14-07-2021.

[7] S. Stellmer, F. Schreck T. C. Killian, Degenerate quantum gases of strontium, *Annual Review of Cold Atoms and Molecules* p. 1–80 (2014).

[8] S. Stellmer, Degenerate quantum gases of strontium, Ph.D. thesis, University of Innsbruck, Innsbruck, Austria (2013).

[9] R. Santra, K. V. Christ C. H. Greene, Properties of metastable alkaline-earth-metal atoms calculated using an accurate effective core potential, *Phys. Rev. A* **69**, 042510 (2004).

[10] H. J. Metcalf P. van der Straten, *Laser Cooling and Trapping* (Springer New York, 1999).

[11] V. S. Letokhov, V. G. Minogin B. D. Pavlik, Cooling and capture of atoms and molecules by a resonant light field, *Soviet Journal of Experimental and Theoretical Physics* **45**, 698 (1977).

[12] J. Mcclelland *et al.*, Bright focused ion beam sources based on laser-cooled atoms, *Applied Physics Reviews* **3** (2015).

[13] J. Sansonetti G. Nave, Wavelengths, transition probabilities, and energy levels for the spectrum of neutral strontium (sr i), *Journal of Physical and Chemical Reference Data* **39**, 033103 (2010).

[14] N. Vaeck, M. Godefroid *et al.*, Multiconfiguration hartree-fock calculations for singlet terms in neutral strontium, *Physical Review A* **38**, 2830 (1988).

[15] C. H. Corliss W. R. Bozman, *Experimental transition probabilities for spectral lines of seventy elements; derived from the NBS Tables of spectral-line intensities* (1962).

[16] S. Saliba R. Scholten, Linewidths below 100 khz with external cavity diode lasers, *Applied Optics* **48**, 6961 (2009).

[17] W. Meinster, The creation of a potassium-40 magneto-optical trap, Master's thesis, University of Amsterdam, Amsterdam, Netherlands (2015).

[18] N. D. Mazumdar, Rebuilding a potassium quantum gas apparatus, Master's thesis, University of Amsterdam, Amsterdam, Netherlands (2016).

[19] E. Hecht, *Optics* (Pearson Education Ltd., Harlow, England, 2017).